Received: 13 April 2025 | Accepted: 22 September 2025

DOI: 10.1111/2041-210X.70181

BRITISH ECOLOGICAL SOCIETY Methods in Ecology and Evolution

RESEARCH ARTICLE

Improving leaf spring phenology modelling for temperate tree species: An integration of the Farquhar–Medlyn photosynthesis model with the optimality-based approach

Yating Gu[1,2] | Zejun Wu[1] | Matteo Detto[3] | Dedi Yang[4] | Jiayue Wang[1] | Yingyi Zhao[1] | Xi Yang[5] | Jin Wu[1,6]

[1]School of Biological Sciences and Institute for Climate and Carbon Neutrality, The University of Hong Kong, Hong Kong, China; [2]Jiangsu Key Laboratory of Soil and Water Processes in Watershed, College of Geography and Remote Sensing, Hohai University, Nanjing, China; [3]Department of Ecology and Evolutionary Biology, Princeton University, Princeton, New Jersey, USA; [4]Environmental Sciences Division and Climate Change Science Institute, Oak Ridge National Laboratory, Oak Ridge, Tennessee, USA; [5]Department of Environmental Sciences, University of Virginia, Charlottesville, Virginia, USA and [6]State Key Laboratory of Agrobiotechnology (CUHK), Hong Kong, China

Correspondence
Jin Wu
Email: jinwu@hku.hk

Funding information
HKU Seed Funding for Strategic Interdisciplinary Research Scheme; Hong Kong Research Grant Council General Research Fund, Grant/Award Number: 17305321; The Innovation and Technology Fund (funding support to State Key Laboratory of Agrobiotechnology); National Natural Science Foundation of China, Grant/Award Number: 31922090; The Office of Biological and Environmental Research in the United States Department of Energy, Office of Science and the Laboratory Directed Research and Development Program of Oak Ridge National Laboratory; Hong Kong Research Grant Council Collaborative Research Fund, Grant/Award Number: C5062-21GF

Handling Editor: Jessica Royles

Abstract

1. Spring leaf phenology in temperate tree species is highly sensitive to climate change and significantly affects plant photosynthetic performance, resource utilization, competition and trophic interactions, thereby impacting various ecosystem functions. Although optimality-based (OPT) approaches for modelling spring phenology are increasingly recognized, the optimal representation of the underlying principle (balancing photosynthesis gains with chilling risks) remains controversial.
2. Here, we integrated a coupled Farquhar–Medlyn photosynthesis model into an existing OPT model, and termed the resulting model R-OPT, and evaluated its performance using the PEP725 dataset, which includes 409,144 site-species-year records from across Europe.
3. Our results show that R-OPT outperforms both the default OPT and non-optimality-based models (e.g. the chilling-forcing trade-off and growing degree day models). This improved performance is consistent within and across five focal tree species but varies by region: R-OPT excels in lowland, moist environments but is less effective in high-altitude, cold, and dry areas, possibly due to an incomplete representation of environmental constraints on photosynthetic carbon gain in these regions.
4. Our research advances leaf spring phenology modelling by emphasizing an optimality principle that balances photosynthetic carbon gain with chilling risk, improving the representation of plant photosynthesis processes and enhancing

Yating Gu and Zejun Wu are co-first author.

understanding of environmental factors influencing phenology in the context of climate change.

KEYWORDS
coupled Farquhar–Medlyn photosynthesis model, maximizing carbon gain, minimizing chilling risk, optimality principle, spring phenology, temperate tree species

1 | INTRODUCTION

Spring leaf phenology (spring phenology hereafter)—the timing of plant leaf emergence and development during spring—plays an important role in regulating plant functions, ecosystem services and biogeochemical feedback related to climate change (Badeck et al., 2004; Lieth, 2013; Piao et al., 2019). Alterations in spring phenology can impact species interactions and cause cascade effects on trophic levels (Chmura et al., 2019; Cohen et al., 2018; Yang & Rudolf, 2010). Shifts in spring phenology, such as earlier spring growth, can extend photosynthetic periods and enhance ecosystem productivity (Buermann et al., 2018; Richardson et al., 2010; Zohner et al., 2021). Spring phenology is also a regulator of seasonal and annual evapotranspiration, the process by which water is transported from land to the atmosphere, and terrestrial albedo, thereby influencing Earth's overall water and energy balance (Cheng et al., 2021; Wang et al., 2019). With climate change driving widespread shifts in phenological patterns, the need for a deeper understanding of the mechanisms regulating phenology has never been more urgent.

In recent decades, advances in understanding the mechanisms and drivers of spring phenology have enabled the development of process-based models that simulate plant seasonal growth and ecosystem carbon and water fluxes within Earth System Models (ESMs; Kolassa et al., 2020). Currently, three primary types of process-based models are used to simulate spring phenology. The first type, known as the one-phase, includes the Growing Degree Day (GDD) model, which posits that leaf unfolding date (LUD) occurs when accumulated GDD surpasses a certain threshold (McMaster & Wilhelm, 1997; Wang et al., 2020). This model, which depends solely on temperature, overlooks the complexity of processes regulating leaf emergence, leading to significant biases in phenology predictions (Piao et al., 2019; Wang et al., 2020). In response to evidence showing that leaf phenology is controlled by both endodormancy (chilling-dominant) and ecodormancy (forcing-dominant), two-phase models have been developed (Chuine, 2000; Lundell et al., 2020; Sapkota et al., 2023). While these models are more accurate and complex, they depend on phenomenological species-specific chilling and forcing functions (Mo et al., 2023), and the relationship between the two phases—whether parallel (Wang et al., 2023) or sequential (Kim et al., 2022)—remains debated, hindering their broader application (Wang et al., 2020). The third type is the optimality-based (OPT) model, which frames spring phenology as a trade-off between maximizing potential photosynthesis gain and minimizing potential early growing-period chilling/frost damage.

There is a growing consensus that OPT approaches are superior for modelling spring phenology in temperate regions, and these models have consistently outperformed other process-based models in predicting spring phenology, as evaluated in both field and remote sensing observations (Gu et al., 2023; Meng et al., 2021). However, the OPT model still exhibits considerable model residuals, probably due to incomplete mechanisms, and faces key limitations that need addressing. For example, Gu et al. (2023, 2025) found that the current OPT model's residuals across temperate ecosystems are not random but exhibit a strong dependency on light and vapour pressure deficit (VPD)—factors that suggest an incomplete representation of plant photosynthesis.

Mechanistically, if spring phenology is subject to the fundamental trade-off between potential carbon gain and chilling damage risk, then models that explicitly account for factors affecting net photosynthetic uptake should impose more effective constraints than those relying solely on photoperiod and forcing components used in the current OPT model (e.g., Descals et al., 2022). Our current knowledge in modelling photosynthesis and the availability of long-term fine-scale phenological datasets presents a unique opportunity to test this hypothesis. For example, the coupled Farquhar–Medlyn model, which integrates a biochemical-based photosynthesis model (Farquhar et al., 1980) with an optimality-based stomatal conductance model (Medlyn et al., 2011), enables the simulation of plant photosynthetic rates, accounting for both biochemical constraints on plant photosynthesis and environmental stimuli on stomatal regulation. The model has been extensively evaluated and proven effective in simulating plant photosynthesis (Guo et al., 2022; Wu et al., 2017). Importantly, this coupled model allows for a more comprehensive set of environmental factors and plant traits to be included in the phenological framework (e.g. temperature, humidity, atmospheric pressure, ambient CO_2 level), thereby enabling the predictions of the effect of new climate scenarios on phenological patterns.

This study investigates whether current approaches to spring phenology lack the mechanistic basis needed to interpret responses to environmental variability and predict the consequences of climate change on phenological patterns. We address this question by incorporating the coupled Farquhar–Medlyn photosynthesis model into the existing OPT approach (Meng et al., 2021), thereby enabling a mechanistic representation of environmental factors

and plant functional traits in phenological models. Specifically, we focus on three research objectives: (1) to assess whether integrating the coupled Farquhar–Medlyn photosynthesis model with the OPT framework can enhance the process modelling of spring phenology compared to existing methods (OPT and non-OPT-based models); (2) to determine whether cross-model comparison results are consistent both within and across different temperate tree species; (3) to explore whether cross-model comparison results are consistent across various background climate conditions, aiming to infer the appropriate scenarios for the application of each approach. To accomplish our objectives, we utilize the Pan European Phenology Network phenology dataset (PEP725, www.pep725.eu), which includes over 409,144 site-species-year records from 1958 to 2016, covering five species and spanning 14 European countries. This dataset offers a unique resource for comprehensive model assessments and cross-comparisons across biotic and abiotic scenarios, including diverse plant species, extensive environmental gradients and prolonged time spans (Gallinat et al., 2021; Schrodt et al., 2020).

2 | MATERIALS AND METHODS

2.1 | Study area

The study area is located in Central Europe, primarily encompassing Austria, Germany and Switzerland. This domain extends from 40°N to 70°N in latitude and 10°W to 30°E in longitude (Figure 1). The area exhibits significant altitude variations, ranging from 0 to 1200 m a.s.l., mostly related to the Alpine chain in the southern part of the domain. We selected this region as our study area for two main reasons: (1) the PEP725 provides long-term, consistent, high-quality records on phenological events such as the beginning of flowering, fruits ripe for picking, leaf unfolding and first leaves separated, enabling effective model evaluation at the species level over the past few decades (Templ et al., 2018; Tian et al., 2021); and (2) the diverse environmental conditions associated with latitude, longitude and altitude present sufficient variability to assess the effectiveness and applicability of our proposed model (Cook et al., 2012; Meng et al., 2021).

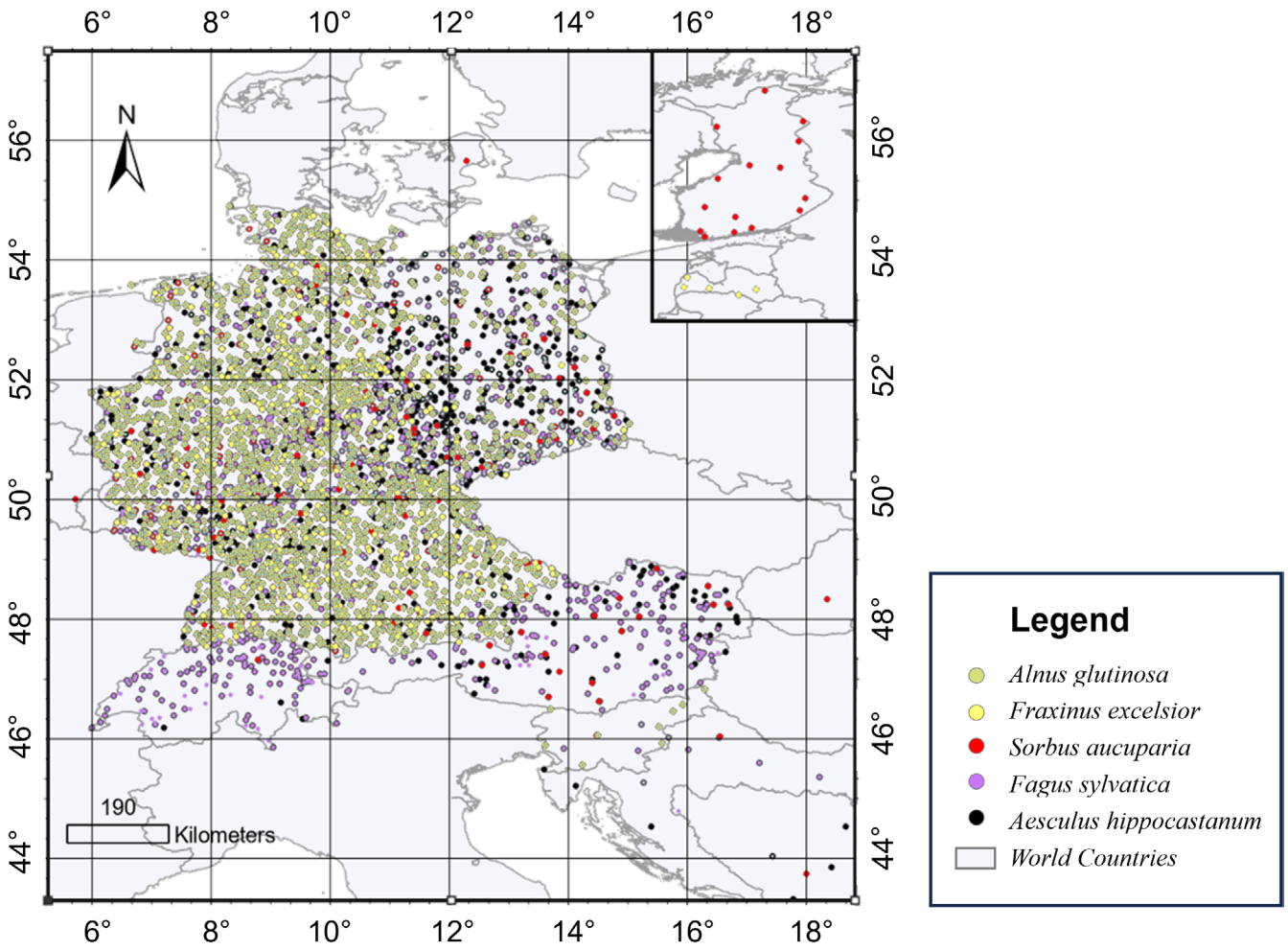

FIGURE 1 Study sites within the PEP725 network. This study focuses on five species from the PEP725 network that have extensive spatial coverage and abundant data records: *Sorbus aucuparia*, *Fagus sylvatica*, *Aesculus hippocastanum*, *Alnus glutinosa* and *Fraxinus excelsior*. These species are primarily distributed across Central Europe, including Austria, Germany and Switzerland.

2.2 | Materials

In this study, we utilized two types of data. The first type consists of ground-based phenology observations from the PEP725 dataset. The second type comprises environmental variable data, which were extracted using the Google Earth Engine (GEE) platform. We provide detailed information on these two data sources as follows.

2.2.1 | Phenological data

Ground observations of key phenological dates, including leaf unfolding dates, for various species in deciduous broadleaf forests have been recorded in the PEP725 database since 1958 (Scheifinger et al., 2018). Since our study focuses on spring phenology modelling, we extracted the leaf unfolding date information from the PEP725 database, which is defined as the date when either the first leaf unfolds or the first visible leaf stalk appears based on BBCH code (Biologische Bundesanstalt, Bundessortenamt und Chemische Industrie, BBCH = 11) (Templ et al., 2018). To provide a sufficient time frame for training and evaluating process-based models, we retained only leaf-out date observations with at least 30 years of data at each site between 1958 and 2016. Based on this criterion, we further selected five primary species of deciduous broadleaf trees for analysis: *Sorbus aucuparia* ($n = 25{,}844$), *Fagus sylvatica* ($n = 108{,}561$), *Aesculus hippocastanum* ($n = 134{,}202$), *Alnus glutinosa* ($n = 68{,}321$) and *Fraxinus excelsior* ($n = 72{,}216$). These five species have the most comprehensive records during the study period and have been widely used in many phenological studies (Fu et al., 2019; Meng et al., 2021). In total, our analysis used 409,144 individual observations from 12,958 site–species combinations at 4232 sites. This extensive dataset allowed us to conduct a thorough investigation of factors influencing leaf-out dates across various tree species and regions.

2.2.2 | Environmental data

To drive the process-based spring phenology models and assess potential use conditions for each model, we extracted key environmental variables for each plant individual with phenological observations at the site level. These variables were obtained from the ERA5-Land Hourly dataset-ECMWF Climate Reanalysis using GEE on a daily timescale (https://developers.google.com/earth-engine/datasets/catalog/ECMWF_ERA5_LAND_HOURLY). This dataset has been produced by reanalysing the land component of the ECMWF ERA5 climate and combining model data with global ground observations, providing a consistent measure of temporal dynamics in key environmental variables since 1950. By matching each phenological station to a specific grid based on its latitude and longitude, we further extracted daily mean temperature (T) and air pressure (P) from the ERA5-Land dataset and resampled them to a 9 km spatial resolution for model simulation. In addition to this, we extracted daily dew point temperature and relative humidity (%) from the ERA5-Land dataset, along with daily temperature and air pressure, to calculate vapour pressure deficit (VPD) following Yuan et al. (2019). We also approximated the photosynthetic photon flux density (PPFD) from the daily solar radiation in the ERA5-Land dataset using the following conversion:

$$1\frac{\mathrm{W}}{\mathrm{m}^2} \approx 4.6\frac{\mu\mathrm{mol}}{\mathrm{m}^2\mathrm{s}} \tag{1}$$

Additionally, we extracted daily CO_2 data from the Mauna Loa Observatory (https://gml.noaa.gov/webdata/ccgg/trends/co2/co2_daily_mlo.txt). However, as daily records were only available from 19 May 1974 onwards, we substituted the daily CO_2 data prior to this date with monthly mean values. While recent studies have shown significant spatial heterogeneity in atmospheric CO_2 across the Earth's surface, this variability is smaller than the temporal changes in atmospheric CO_2 level, especially over a time duration exceeding 30 years (like in our study). Consequently, we believe that using CO_2 data from the Mauna Loa Observatory to approximate the temporal CO_2 level dynamics in our study area would introduce limited uncertainty in spring phenology modelling.

We calculated Daylength (L) as a function of latitude and the day of the year following the equations as proposed by Forsythe et al. (1995):

$$L = 24 - \frac{24}{\pi}\times\cos^{-1}\left(\frac{\sin\frac{0.8333\pi}{180} + \sin\frac{\pi}{180}\sin\varphi}{\cos\frac{L\pi}{180}\times\cos\varphi}\right) \tag{2a}$$

$$\varphi = \sin^{-1}(0.39795\times\cos\theta) \tag{2b}$$

$$\theta = 0.2163108 + 2\tan^{-1}(0.9671396\times\tan(0.0086\times(\mathrm{DOY}-186))) \tag{2c}$$

where φ and θ are the sun's declination and revolution angles, respectively, both measured in radians.

2.3 | Data analysis

In this study, we developed a novel spring phenology model (R-OPT) that combines the optimality-based principle, as employed in Meng et al. (2021), with a process-based photosynthesis model, specifically the coupled Farquhar–Medlyn photosynthesis model (Guo et al., 2022; Wu et al., 2017). We evaluated the performance of the R-OPT model using the benchmark phenology dataset from PEP725 and conducted a comparative analysis with existing process-based spring phenology models: the Growing Degree Day model (GDD), the chilling-forcing trade-off model (CFT) and the optimality-based model (OPT). Through this comprehensive analysis, we aimed to provide a rigorous evaluation of our proposed R-OPT model, showcasing its advantages and identifying appropriate use conditions in comparison to existing process-based models.

2.3.1 | Four phenological models

Here, we examined four phenological models, with their detailed formulas and underlying hypotheses summarized in Table 1 and the specific model equations along with the parameter settings being provided in the Supporting Information.

The first model, GDD, is temperature-dependent and calculates a plant's accumulated heat requirement to infer leaf-out dates. In this model, LUD occurs when growing degree days exceed a specific heat requirement threshold (Table 1a; Equations 3 and 4).

$$R_{f,i} = \begin{cases} 0, & T_i \le T_{\text{base}} \\ T_i - T_{\text{base}} & T_i > T_{\text{base}} \end{cases} \quad (3)$$

$$F_t = \sum_{i=t_0}^{t} R_{f,i} \quad (4)$$

where $T_{\text{base}} = 5°C$ is the temperature threshold for biological activity, $R_{f,i}$ is the daily rate of forcing, and F_t is the accumulated forcing from t_0 (empirically set as the first day of the calendar year) to day t. Leaf-out is predicted to occur on the first day i for which the cumulative forcing F_t (Equation 4) meets or exceeds the critical threshold F_{thres}; that is $F_t \ge F_{\text{thres}}$.

The second model, CFT, builds upon the GDD model by incorporating both chilling and forcing processes as constraints on LUD. CFT posits that trees begin accumulating chilling and forcing from winter, with the onset of spring leaf-out being predicted when forcing accumulation exceeds a threshold set by chilling accumulation. Consequently, LUD is determined by the interplay between temperature effects on chilling (represented by a triangular function) and forcing (represented by a sigmoid function) (Table 1b; Equations 5–8).

$$R_{c,i} = \begin{cases} 0 & T_i < T_{\min} \\ \dfrac{T_i - T_{\min}}{T_{\text{opt}} - T_{\min}} & T_{\min} \le T_i < T_{\text{opt}} \\ \dfrac{T_i - T_{\text{opt}}}{T_{\max} - T_{\text{opt}}} & T_{\text{opt}} \le T_i < T_{\max} \\ 0 & T_i > T_{\max} \end{cases} \quad (5)$$

$$R_{f,i} = \begin{cases} 0, & T_i \le T_{\text{base}} \\ \dfrac{28.4}{1+\exp(3.4-0.185T_i)} & T_i > T_{\text{base}} \end{cases} \quad (6)$$

$$C_t = \sum_{i=t_0}^{t} R_{c,i} \quad (7)$$

$$F_t = \sum_{i=t_0}^{t} R_{f,i} \quad (8)$$

where T_i is the average temperature on the ith day; $T_{\min} = -5°C$, $T_{\text{opt}} = 10°C$ and $T_{\max} = 25°C$ are set constants based on (Wang et al., 2020). $R_{f,i}$ is the daily rate of forcing and $R_{c,i}$ is the daily rate of chilling. C_t and F_t are the accumulated chilling and forcing from t_0 (empirically set as the first day of the calendar year) to day t. The model includes two fitting parameters: a and b. Leaf-out is predicted to occur on the first day i when the accumulated forcing F_t (Equation 8) meets or exceeds the threshold ae^{-bC_t}; that is, when $F_t \ge ae^{-bC_t}$. This criterion reflects the balance between the accumulation of forcing required for leaf development and the mitigating effect of accumulated chilling, which reduces the risk of frost damage.

The third model, OPT, expands on the CFT model by further incorporating a chilling-dependent photoperiod variable (Meng et al., 2021). This modification considers the influence of photoperiod on the efficiency of forcing accumulation, which is

TABLE 1 The formula of four representative spring phenology models.

No.	Models	Hypothesis	Input	Number of parameters	References
a	GDD	LUD is triggered when the cumulative heat unit exceeds a base temperature	T	1	De Réaumur (1735)
b	CFT	LUD is triggered by the interaction between chilling and forcing	CF	2	Hänninen (1990)
c	OPT	LUD is triggered by the trade-off between minimizing chilling risk while maximizing early-season photosynthesis potential gain (approximated by forcing and photoperiod)	CFP	3	Meng et al. (2021)
d	R-OPT	LUD is triggered by the trade-off between minimizing chilling risk while maximizing early-season photosynthesis potential gain (approximated by Farquhar–Medlyn photosynthesis model)	CG	3	Farquhar et al. (1980), Gu et al. (2023) and Medlyn et al. (2011)

Note: For abbreviation letters in 'Input' aspect: C, chilling temperature; F, forcing temperature; G, carbon gain responses by photosynthesis; P, photoperiod; T, temperature responses are not separable in chilling or forcing. The mathematical formula is provided in the Supporting Information.

chilling-dependent (e.g., a strong photoperiod effect under low chilling; Caffarra et al., 2011). The OPT model is grounded in the hypothesis that the timing of LUD reflects a plant's strategy to optimize potential photosynthetic carbon gain while minimizing chilling risk. Detailed information about this model can be found in Table 1c (Equations 9–13).

$$R_{c,i} = \begin{cases} 0 & T_i < T_{\min} \\ \dfrac{T_i - T_{\min}}{T_{\text{opt}} - T_{\min}} & T_{\min} \le T_i < T_{\text{opt}} \\ \dfrac{T_i - T_{\text{opt}}}{T_{\max} - T_{\text{opt}}} & T_{\text{opt}} \le T_i < T_{\max} \\ 0 & T_i > T_{\max} \end{cases} \quad (9)$$

$$R_{f,i} = \begin{cases} 0, & T_i \le T_{\text{base}} \\ \dfrac{28.4}{1+\exp(3.4-0.185T_i)} & T_i > T_{\text{base}} \end{cases} \quad (10)$$

$$R_{p,i} = \frac{L_i}{12} e^{-cR_{c,i}} \quad (11)$$

$$C_t = \sum_{i=t_0}^{t} R_{c,i} \quad (12)$$

$$F_t = \sum_{i=t_0}^{t} R_{f,i} \times R_{p,i} \quad (13)$$

where T_i is the average temperature of the ith day; $T_{\min}$ = −5°C, T_{opt} = 10°C, and $T_{\max}$ = 25°C are set as constants based on (Wang et al., 2020). $R_{f,i}$ is the daily rate of forcing, $R_{c,i}$ is the daily rate of chilling, and $R_{p,i}$ the state of realized forcing (Meng et al., 2021). L_i is the day length on the ith day, and C_t and F_t are the accumulated chilling and forcing from t_0 (empirically set as the first day of the calendar year) to t. The model includes three fitting parameters: a, b, and c. Leaf-out is predicted to occur on the first day i when the accumulated realized forcing for potential photosynthetic carbon gain, F_t (Equation 13), meets or exceeds the threshold e^{-bC_t}; that is, when $F_t \ge ae^{-bC_t}$. This criterion reflects that LUD is determined by the point at which the benefits of potential photosynthetic carbon uptake surpass the potential negative impact associated with frost damage risk.

The final model, or revised OPT (R-OPT), builds upon the OPT model and the modification (Table 1d) is based on two primary principles. First, it maintains the fundamental hypothesis of the OPT model, which considers spring phenology as a trade-off between potential chilling risk (Equations 14 and 15) and potential carbon gain (Equations 16–18). Second, the use of a mechanistic-based approach for representing photosynthesis, as opposed to the photoperiod and forcing components employed by Meng et al. (2021), allows for a more accurate simulation of photosynthesis. This enables direct testing of the role of potential photosynthesis gain in mediating spring phenology and incorporates additional environmental variables (e.g. light, CO_2 and humidity) that have been previously identified as important regulators of spring phenology variability (Gu et al., 2023; Gu et al., 2025). Specifically, we used the coupled Farquhar (Farquhar et al., 1980)–Medlyn (Medlyn et al., 2011) photosynthesis model with average daily climate variables as inputs (Equation 16), which has been extensively evaluated with demonstrated accuracy in several studies (e.g., Guo et al., 2022; Wu et al., 2017).

$$R_{c,i} = \begin{cases} 0 & T_i < T_{\min} \\ \dfrac{T_i - T_{\min}}{T_{\text{opt}} - T_{\min}} & T_{\min} \le T_i < T_{\text{opt}} \\ \dfrac{T_i - T_{\text{opt}}}{T_{\max} - T_{\text{opt}}} & T_{\text{opt}} \le T_i < T_{\max} \\ 0 & T_i > T_{\max} \end{cases} \quad (14)$$

$$C_t = \sum_{i=t_0}^{t} R_{c,i} \quad (15)$$

$$R_{f,i} = \text{Photosyn}(A_n, g_s) \quad (16)$$

$$R_{p,i} = \frac{L_i}{12} e^{-cR_{c,i}} \quad (17)$$

$$F_t = \sum_{i=t_0}^{t} R_{f,i} \times R_{p,i} \quad (18)$$

In this modelling context, T_i is the average temperature of the ith day; $T_{\min}$ = −5°C, T_{opt} = 10°C, and $T_{\max}$ = 25°C are set constants based on (Wang et al., 2020). $R_{f,i}$ is the daily rate of simulated photosynthesis, $R_{c,i}$ is the daily rate of chilling and $R_{p,i}$ the state of realized forcing (Meng et al., 2021). L_i is the day length on the ith day, and C_t and F_t are the accumulated chilling and forcing from t_0 (empirically set as the first day of the calendar year) to t. The model has three fitting parameters: a, b and c. Leaf-out is predicted to occur on the first day i when the accumulated realized forcing for potential photosynthetic carbon gain, F_t (Equation 18), equals or exceeds the threshold a ae^{-bC_t}; that is, when $F_t \ge ae^{-bC_t}$. This criterion also indicates that LUD is determined by the point at which the potential photosynthetic carbon benefit surpasses the potential negative impact associated with frost damage risk.

The Photosyn function is a coupled model, defined as $R_{f,i} = \text{Photosyn}(A_n, g_s)$, which integrates the Farquhar–Medlyn model of photosynthesis (A_n) and the stomatal conductance model (g_s). This function incorporates multiple environmental factors as inputs to calculate the leaf net photosynthesis rate (Figure S2). The Photosyn function returns the hyperbolic minimum of V_{cmax} and $J_{\max}$-limited photosynthetic rates, as well as the hyperbolic minimum of $J_{\max}$-limited and TPU-limited rates. When the intercellular CO_2 concentration (C_i) is not provided, it can be determined by finding the intersection between the CO_2 'supply' (governed by the Medlyn stomatal conductance model) and 'demand' (defined by the Farquhar photosynthesis model). The detailed formula is as follows:

$$A_n = \min(A_c, A_j, A_p) - R_d \quad (19)$$

$$g_s = g_0 + 1.6 \times \left(1 + \frac{g_1}{\sqrt{\text{VPD}}}\right) \times \frac{A_n}{C_a} \quad (20)$$

where A_c is the Rubisco-limited rate (parameterized by maximum carboxylation rate at a reference temperature of 25°, $V_{c,\max 25}$, in μmol CO_2 $m^{-2}s^{-1}$); A_j is the RuBP regeneration-limited rate (in μmol CO_2 $m^{-2}s^{-1}$); A_p is the triose phosphate utilization (TPU)-limited rate (in μmol CO_2 $m^{-2}s^{-1}$), and R_d represents CO_2 evolution from mitochondria in the presence of light (in μmol CO_2 $m^{-2}s^{-1}$). Additionally, g_0 refers to the residual conductance to water vapour (in mol $m^{-2}s^{-1}$); VPD is short for vapour pressure deficit (in kPa) and g_1 is the stomatal slope; and C_a is the atmospheric CO_2 concentration (in ppm).

Although there are considerable variations in $V_{c,\max 25}$ and g_1 across species and growing environments (Yan et al., 2023), we set $V_{c,\max 25}$ to a constant of 65 μmol $m^{-2}s^{-1}$ and g_1 to a constant of 3.12 based on observations in (Medlyn et al., 2002) and (Atkin et al., 2015; Lin et al., 2015), respectively. Our additional sensitivity test demonstrates that the assigned $V_{c,\max 25}$ as well as g_1 value has a negligible effect on the performance of our R-OPT model at the site-species level (Figure S1), thus minimally impacting our hypothesis testing (i.e. whether the use of the Farquhar–Medlyn photosynthesis model would improve photosynthesis representation and, consequently, enhance the process-based phenology modelling). Further detailed information about this photosynthesis model, including the formulations of other parameters (e.g. $J_{\max}$ and R_d) and temperature-dependent functions can be found in Tables S1 and S2.

After simulating photosynthesis using this coupled Farquhar–Medlyn model, driven by real-world environmental variables, including light, temperature, vapour pressure deficit, atmospheric pressure and atmospheric CO_2, we replaced the corresponding F_t (Equation 13) modelled by photoperiod and forcing in the original OPT model with that (i.e. Equation 18) inferred from the Farquhar–Medlyn model.

2.3.2 | Model fitting and cross-validation

In this study, we employed a repeated fivefold cross-validation method to train and calibrate each model for each species on a site-by-site basis (Yan et al., 2021). We employed root mean squared error (RMSE) for model performance evaluation. The training process was designed to minimize RMSE between the model's predictions and the field-observed LUD for each site-species combination throughout the decadal time series. Specifically, for each site-species, we randomly divided the full dataset into calibration and independent validation subsets, using a fivefold cross-validation, and repeated the whole process 20 times. Given that each site had a data record spanning approximately 30–60 years for each species, we selected the mean calibrated parameters for subsequent prediction processes. This cross-validation method allowed us to estimate how well the model performed on unseen data with a given set of parameters (Table 1), aiding in parameter tuning, assessing the impact of parameter variations on model performance, and comparing models with different complexity. Subsequently, we applied a *t*-test to assess whether the population distribution of the RMSE difference between each model pair across all site-species combinations was statistically significant (Wu et al., 2020).

In addition to aggregating all site-species data, we conducted a comparative assessment to further evaluate the statistical significance of the relative improvement between different process-based models. This involved calculating the accuracy differences between each pair of models for every site-species and deriving the histogram distribution of the model performance difference for each model pair. We also compared these differences with key environmental variables, including altitude, mean annual temperature (MAT) and mean annual precipitation (MAP). Through this analysis, we aimed to understand the appropriate use conditions for each of the analysed models.

3 | RESULTS

3.1 | Evaluation of process-based phenological model performance both within and across temperate tree species

In our cross-comparison of the four process-based models (i.e. GDD, CFT, OPT and R-OPT) for spring phenology modelling, we found that overall, the R-OPT model performed the best. While it performed slightly better than OPT, it significantly outperformed GDD and CFT (Figure 2). This observation remained consistent regardless of whether the data analysis was performed across all species or at a species-specific level. For instance, the analysis at the species level showed that the R-OPT model yielded a median RMSE of 7.61 days across all species and all sites. This surpassed the OPT, GDD and CFT models, which had median RMSEs of 7.91, 8.97 and 8.99 days, respectively (Figure 2a). Similar findings regarding the relative model performance ranking were also observed at the species level (Figure 2b–f), but with some exceptions. For the species *Sorbus* (Figure 2b) and *Fraxinus* (Figure 2f), GDD performed better than CFT, while in *Fraxinus*, OPT slightly outperformed R-OPT (Figure 2f).

Our results in Figure 3 support our interpretation of Figure 2 in a more rigorous statistical manner, with consistent findings regardless of the model performance metric used or the level of analysis conducted at the species or all species level. Considering the all species level analysis, our results show that R-OPT significantly outperforms OPT, both of which are three-parameter models. This improvement is evidenced by a reduction in RMSE for 68.66% of all site-species combinations (Figure 3a), resulting in a median decrease of 0.25 days (Figure 2a). Although modest in absolute terms, this reduction is meaningful given the daily resolution of phenological predictions and the sensitivity of ecosystem processes to spring onset timing. OPT substantially outperforms CFT, with 97.16% of

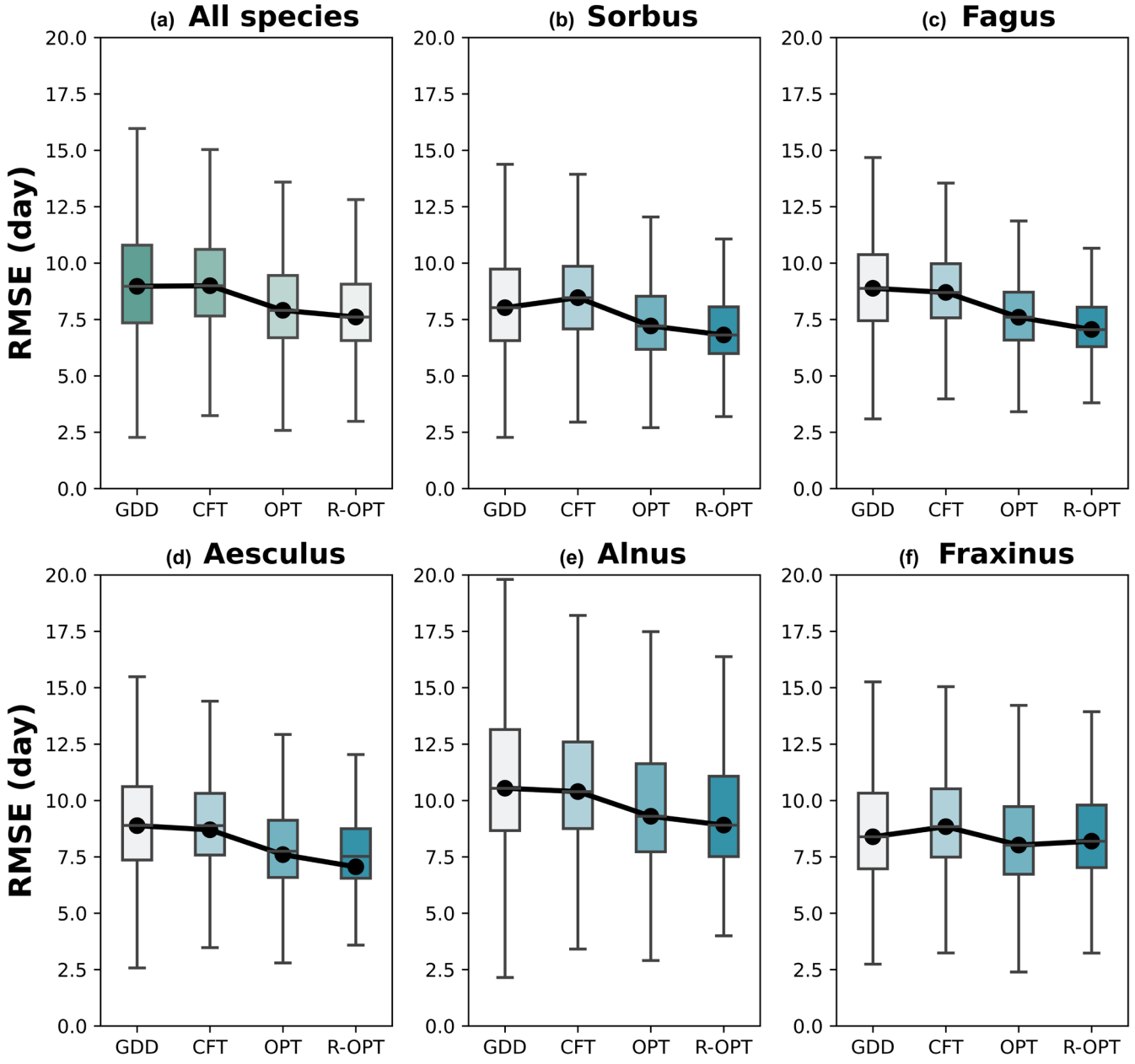

FIGURE 2 Performance comparison of the four process-based models in spring phenology modelling, evaluated using RMSE obtained from the fivefold cross-validation. Model performance was assessed both across all species ($n = 4193$ site-species; a) and at the species-specific level for *Sorbus* ($n = 1186$ sites; b), *Fagus* ($n = 3402$ sites; c), *Aesculus* ($n = 3994$ sites; d), *Alnus* ($n = 2336$ sites; e), and *Fraxinus* ($n = 2383$ sites; f).

all site-species displaying reduced RMSE, while CFT slightly outperforms GDD, with 60.22% of all site-species exhibiting improvements (Figure 3a). At the species level, we observed a generally similar pattern to the all species analysis, with some differences. For the R-OPT vs. OPT pair, despite consistently more (>50%) sites for each target species with model performance improvement in R-OPT relative to OPT, the percentage of sites with model performance improvement varies considerably across different species. *Fagus* holds 84.13% of all examined sites displaying significant model performance improvement in R-OPT (Figure 3c), while *Fraxinus* had the least improvement at 66.01% (Figure 3f). Consequently, *Fagus* experienced the highest median RMSE decrease of 0.54 days, followed by *Sorbus* (0.40), *Alnus* (0.39) and *Aesculus* (0.23) (Figure 2). For the OPT-CFT pair, the results are rather consistent across all species. For the CFT-GDD model pair, the results vary considerably across species. *Fagus*, *Aesculus* and *Alnus* show no significant model performance difference between CFT and GDD, with approximately 50% of sites displaying model performance improvement (Figure 3c–e). In contrast, *Sorbus* (64.76%) and *Fraxinus* (67.31%) exhibited significant model performance improvement of CFT relative to GDD, as evident by higher than 60% sites displaying model performance improvements (Figure 3b,f).

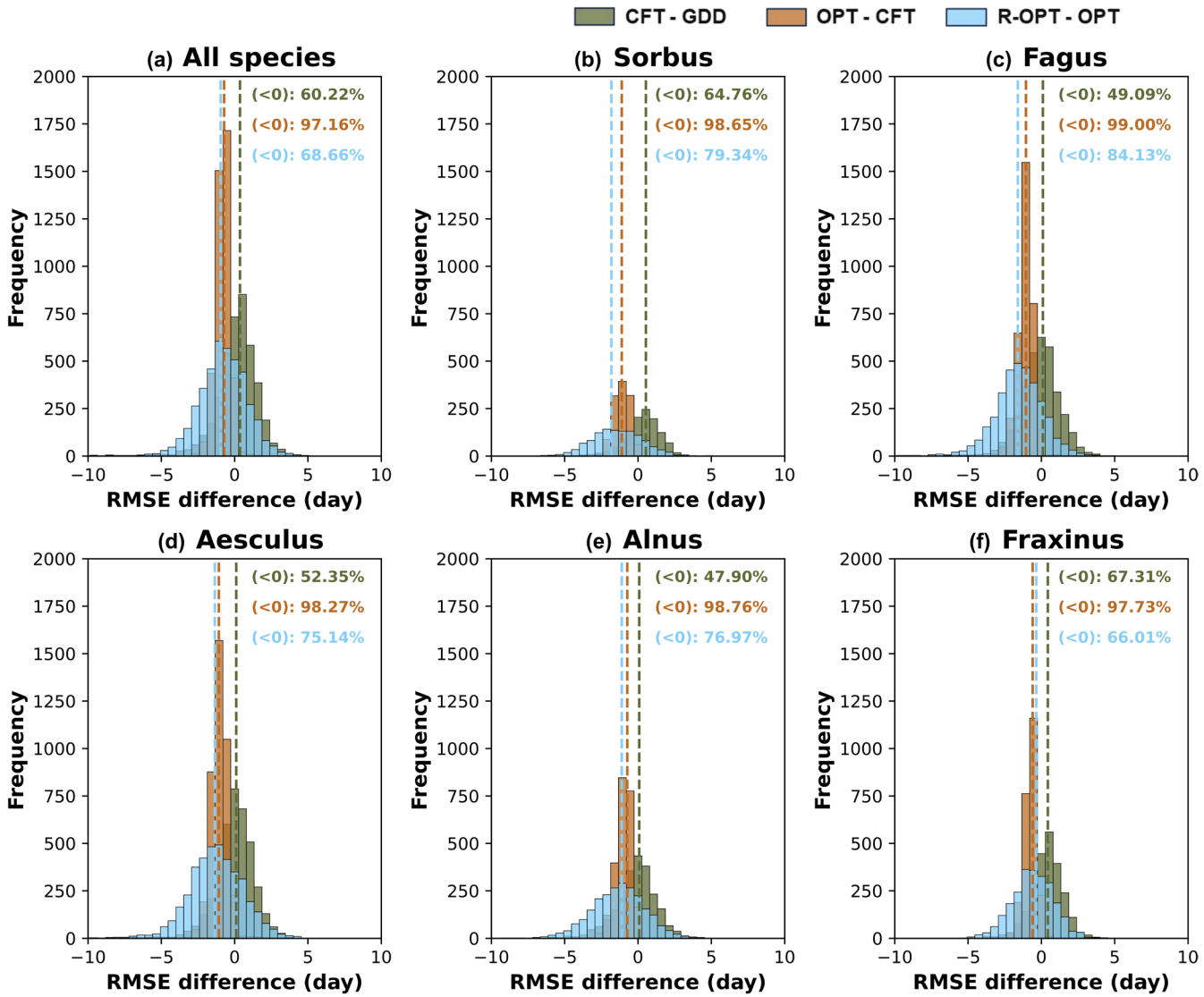

FIGURE 3 Histogram analysis of paired model performance differences using RMSE. Model performance differences were assessed both across all species (a) and at the species level for *Sorbus* ($n = 1186$ sites; b), *Fagus* ($n = 3402$ sites; c), *Aesculus* ($n = 3994$ sites; d), *Alnus* ($n = 2336$ sites; e) and *Fraxinus* ($n = 2383$ sites; f). Notably, 'CFT-GDD' represents the paired model performance difference between CFT and GDD (or the performance metric of CFT minus that of GDD); similar analysis also applies to 'OPT-CFT' (the performance metric of OPT minus that of CFT) and 'R-OPT-OPT' (the performance metric of R-OPT minus that of OPT).

3.2 | Exploring spatial patterns in paired model performance differences across species

Building on the previous histogram analysis, we next delved deeper into the consistency of performance discrepancies across different process-based models within our study region. This investigation was facilitated by categorizing the site-level paired model performance difference (indicated by the difference in model RMSE) into seven cases, as illustrated in Figure 4's legend. These include a neutral state defined by a paired model difference within the range of −1 to 1 day, three significant model performance improvements marked by a negative RMSE difference smaller than 1 day, and three significant model performance reductions indicated by a positive RMSE difference larger than 1 day. Changes within the neutral state were deemed negligible for this analysis.

Upon excluding the neutral range, a comparison between the R-OPT and OPT models revealed a significant enhancement (Figure 4a,d,g,j,m). All species, except *Fraxinus*, demonstrated a competitive performance boost in the R-OPT model, as evidenced by substantially higher site percentages within the three improvement cases (*Sorbus*, 30.35%; *Fagus*, 31.42%; *Aesculus*, 28.11%; *Alnus*, 33.36%; in red) compared to the corresponding percentage within the three reduction cases (*Sorbus*, 15.43%; *Fagus*, 12.23%; *Aesculus*, 20.81%; *Alnus*, 17.85%; in blue). Notably, these model performance differences are not homogeneous across the study region; instead, they show strong spatial heterogeneity, with

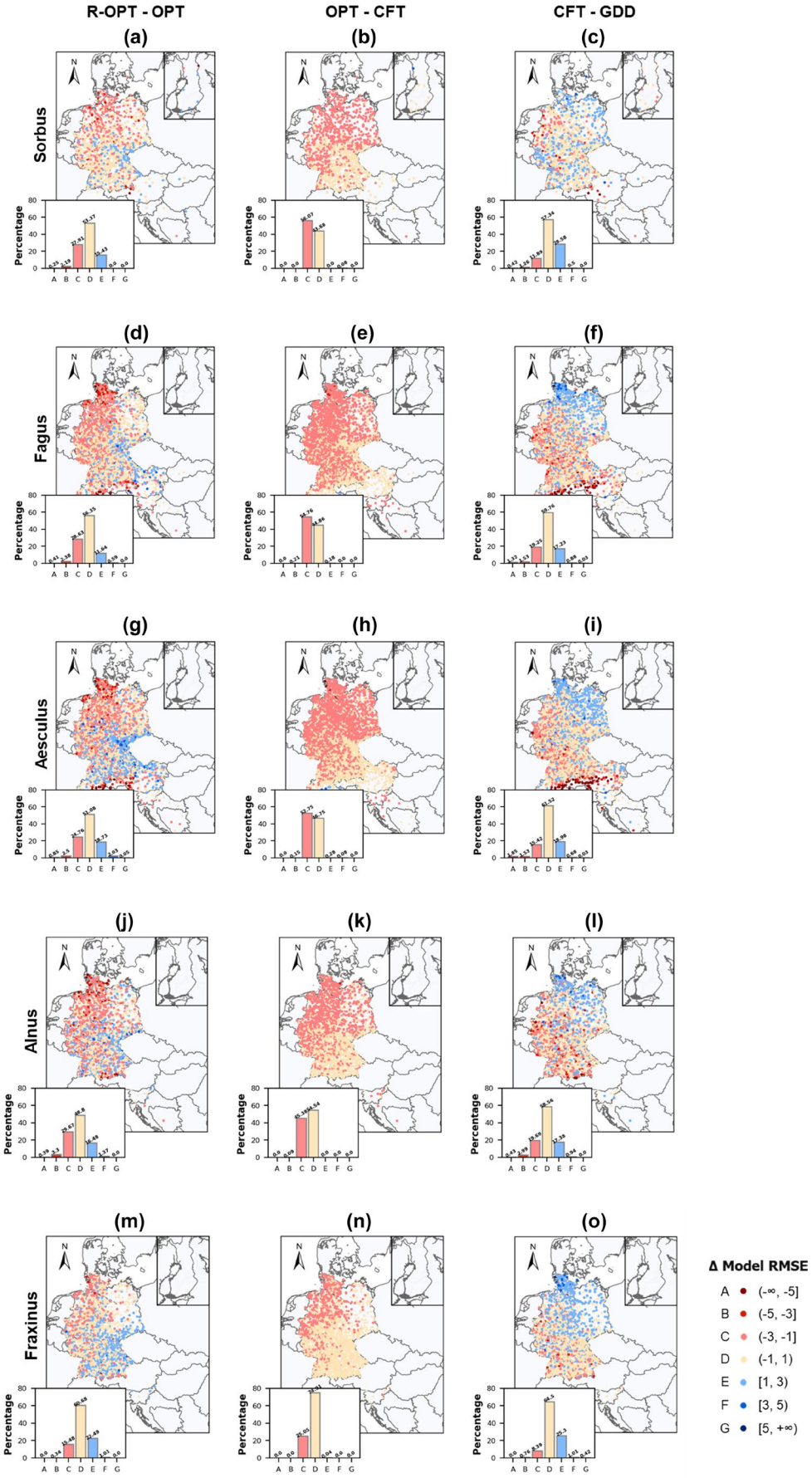

FIGURE 4 Paired model performance differences between different process-based models (R-OPT-OPT; OPT-CFT; CFT-GDD) are examined respectively for *Sorbus* (a–c), *Fagus* (d–f), *Aesculus* (g–i), *Alnus* (j–l) and *Fraxinus* (m–o). The model performance metric of RMSE is used here, and the model RMSE difference (days) are categorized into seven different cases: (−∞, −5], (−5, −3], (−3, −1], (−1, 1), [1, 3), [3, 5), [5, +∞). Red colours indicate increased model performance and blue colours indicate reduced model performance.

improvements dominating the northern and western sites of the study region and reductions dominating the southern and eastern sites. Interestingly, the most substantial enhancements, depicted in dark red, were found at the extreme north and south of our European sites.

Focusing on the OPT–CFT pair, model performance differences were more pronounced (Figure 4b,e,h,k,n). Excluding the neutral state, nearly all the remaining sites across all species experienced model improvement (*Sorbus*, 56.07%; *Fagus*, 54.97%; *Aesculus*, 52.90%; *Alnus*, 45.47%; *Fraxinus*, 25.05%; in red), highlighting the significant effectiveness of the OPT model in characterizing spring phenology over the CFT model. Notably, these enhancements were predominantly concentrated in the northern sites of our study region, with neutral states observed in the southern sites.

Lastly, when examining the CFT-GDD pair, we found that the neutral state dominated the entire study region (with site percentage greater than 50%), with approximately an equal proportion of sites showing either improvement or reduction (Figure 4c,f,i,l,o). This observation was nearly consistent across all five species examined. Notably, the CFT model demonstrated superior performance in the southern sites of our study region and inferior performance in the northern sites.

3.3 | Examining the impact of altitude, precipitation and temperature on the paired model performance difference between R-OPT and OPT across the entire study region

In our analysis of the four models, we found that the relative performance ranking revealed R-OPT and OPT to be on par with each other, both significantly outperforming CFT and GDD (Figures 2 and 3). Furthermore, we noticed strong spatial heterogeneity in the paired model performance difference between R-OPT and OPT (Figure 4). Given these observations, we next shifted our focus to this performance disparity between R-OPT and OPT, examining potential environmental factors contributing to the spatial variation in the R-OPT-OPT paired model performance difference. Our investigation centred on three key environmental variables: altitude (Figure 5a), mean annual precipitation (Figure 5b) and mean annual temperature (Figure 5c). We found that these variables exhibited moderate-to-strong spatial heterogeneity within our study area, characterized by low altitude in the northern sites and high altitude in the southern sites. Precipitation patterns were found to be similar to altitude, while temperature—influenced by the interplay of altitude, precipitation and latitude—displayed less spatial heterogeneity throughout the study region.

Upon examining the influence of altitude on the paired model performance difference, we discovered that the R-OPT model significantly outperforms the OPT model at lower altitudes (e.g. ≤300 m, categories A and B) and tends to have neutral or significantly lower performance at higher altitudes. This pattern was consistent both within and across all five species studied (Figure 5a,d,g,j,m,p,s). With regard to the impact of precipitation on the performance difference, the R-OPT model was found to excel over the OPT model under high precipitation conditions (e.g. ≥1600 mm/year, categories F and G) and remain neutral under lower precipitation conditions. This observation was also consistent within and across all five species examined (Figure 5b,e,h,k,n,q,t). The impacts of temperature on the paired model performance difference, however, were complex and non-significant (Figure 5c,f,i,l,o,r,u), likely due to the temperature being a result of multiple environmental factors (e.g. altitude, latitude and precipitation) and thus its impact on the performance difference being more intricate.

4 | DISCUSSION

In this study, we developed a revised optimality-based model (R-OPT) that integrates the mechanistic Farquhar–Medlyn photosynthesis model with the default OPT to improve spring phenology modelling. The integration was assessed using intensive field observations from the Pan European Phenology Network across Central Europe. Our results demonstrate that the newly proposed R-OPT model significantly outperforms two other widely used models (GDD, CFT) and improves the performance of the original OPT model. However, when cross-compared with OPT, we found that this improvement is subject to spatial variability. Specifically, the R-OPT model outperforms OPT in areas with high MAP (≥1600 mm/year) and low altitude (≤300 m), while providing comparable model performance in other areas. These results highlight the importance of including photosynthetic influences in spring phenology modelling and contribute to a deeper understanding of the spatial variability in interactions among plant spring phenological strategies, chilling risks and photosynthetic processes.

We first sought to evaluate the effectiveness of our R-OPT model at the species level, comparing it with the OPT, GDD and CFT models (Figures 2 and 3). Overall, R-OPT performed better than the rest, ranking first, slightly surpassing OPT and significantly excelling at both CFT and GDD. This rank order of model performance can be attributed to the unique mechanisms each model represents. The GDD model, for instance, describes the heat requirement during ecodormancy but neglects the endodormancy process (e.g. chilling requirements) (McMaster & Wilhelm, 1997). In contrast, the CFT

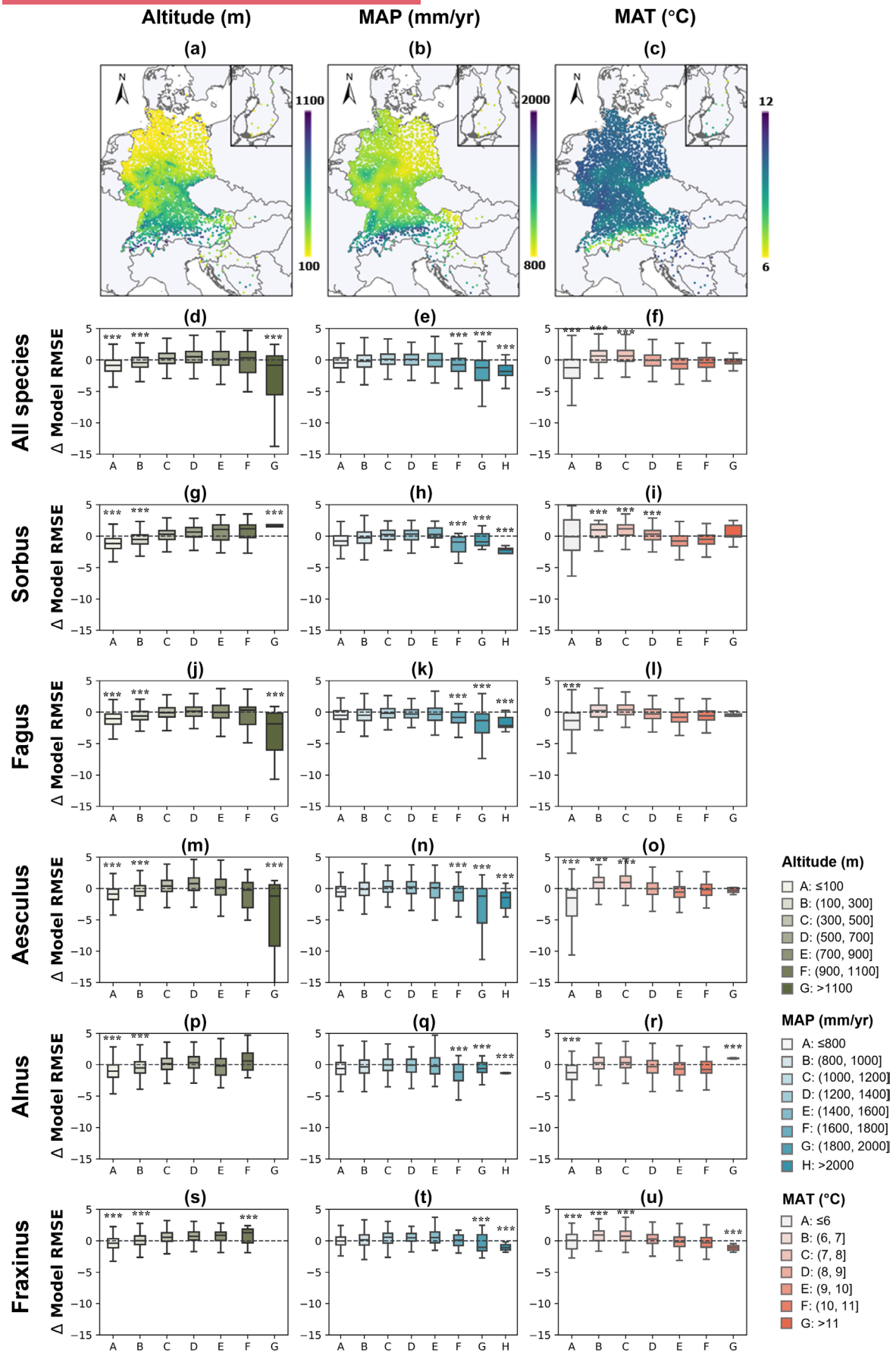

FIGURE 5 Assessing the potential environmental impact on the paired model performance difference between R-OPT and OPT (indicated by the model RMSE difference in days) throughout the entire study region. Panels (a–c) depict the maps of altitude, mean annual temperature (MAT), and mean annual precipitation (MAP) across the study area, respectively. The second to last rows illustrate the impact of each specific environmental factor on the paired model performance difference, both for all species collectively and for individual species, where '***' indicates that the paired model performance difference of that given environmental bin significantly deviates from zero (p-value <0.001). Each column signifies the effect of a particular environmental variable, with the first column (d, g, j, m, p, s) representing altitude, the second column (e, h, k, n, q, t) indicating mean annual precipitation, and the final column (f, i, l, o, r, u) denoting mean annual temperature.

model considers both ecodormancy and endodormancy processes in constraining spring phenology but disregards the potential impact of other environmental factors, such as photoperiod and light intensity (Fang et al., 2024; Wang et al., 2023). These omissions result in the underperformance of GDD and CFT compared to OPT and R-OPT. The significant superiority of OPT over CFT and GDD further supports the interpretation that spring phenology is regulated not only by temperature but also by additional factors such as photoperiod (Meng et al., 2021). The underlying theory of this interpretation posits that spring phenology represents an optimal trade-off between maximizing early growing-season potential plant photosynthetic carbon gain and minimizing potential chilling risks (approximated by temperature) (Fu et al., 2015; Gu et al., 2023). Since light intensity is more effective than photoperiod (used in Meng et al., 2021 for the default OPT model) in approximating early growing-season plant photosynthesis potential (e.g. Gu et al., 2023), and the mechanistic photosynthesis model can consider multiple environmental factors (e.g. light, temperature, CO_2, humidity) that constrain early growing-season plant photosynthesis, it is not surprising that the R-OPT model performs better than OPT. This not only effectively addressed recent issues identified by Gu et al. (2023, 2025), which found light intensity and vapour pressure deficit to be significant contributors to spring phenology model residuals while being under-represented in the original OPT model, but also provides quantitative evidence supporting the view that spring phenology reflects an optimal plant strategy shaped by the fundamental trade-off between potential carbon gain and frost damage risk.

While our R-OPT model consistently demonstrated improved or comparable performance to OPT in most cases examined, there were instances where its performance was less optimal in certain areas compared to OPT (Figure 4). For example, our result indicated that the R-OPT model showed significantly improved performance compared to OPT in low-altitude areas, while the performance difference became neutral or even reversed in high-altitude areas (Figure 5d,g,j,m,p,s). This finding aligns with recent studies that reported the integration of the Farquhar–Medlyn model into land surface models enhances the simulation of carbon and water fluxes in low-altitude forests but not consistently in high-altitude areas (Han et al., 2017; Hernández et al., 2020). The rationale behind this finding could be that montane areas often experience significant diurnal fluctuations in environmental conditions and daylight hours due to topographic effects (Du et al., 2020; Hua et al., 2022). This makes photosynthetic simulations using the mechanistic model challenging without precise data on these fine-scale environmental fluctuations (Prevéy et al., 2017). Another contributing factor could be the necessity for vegetation in montane zones to evolve different strategies for leaf spring phenology regulation to adapt to their colder and harsher environments, including the potential to mitigate the impact of snow cover (Wang et al., 2018; Xie et al., 2021). Further in-depth exploration in this area is needed. Moreover, $V_{c,max25}$ and g_1 could display altitude-dependent variations (Han et al., 2017). Due to a lack of relevant data, we kept these values fixed in our current explorations—an aspect that warrants careful evaluation in future studies. In addition, our results indicated that the phenology of species in higher MAP ranges is better captured by our R-OPT model and tends to be neutral in other MAP ranges (Figure 5f). The underlying reason is likely because abundant MAP can indirectly influence photosynthesis and stomatal conductance by affecting soil moisture and plant water status (Franks et al., 2024; Navarro et al., 2022; Ofori-Amanfo et al., 2020), which can be better captured by the proposed Farquhar–Medlyn photosynthesis model. Conversely, in conditions of insufficient precipitation, plants may close their stomata to conserve water and thus reduce the rate of photosynthesis (Buckley, 2005; Garcia-Forner et al., 2016), which is less well captured by the Medlyn model that has been previously demonstrated to perform well in capturing plant stomatal conductance dynamics under well-water conditions and less well under stress conditions (Anderegg et al., 2017; Wu et al., 2020; Zhou et al., 2013). Future in-depth analysis is also needed in this area.

By improving process-based modelling of spring phenology, our research has significant implications for large-scale Earth System Modelling (ESMs). In ESMs, phenology currently functions as a 'hard' switch that controls the activation and deactivation of key plant physiological processes, including photosynthesis, respiration, transpiration, as well as other essential ecosystem functions linked to phenological transitions (Miller et al., 2023; Nehemy et al., 2023; Piao et al., 2019). However, most ESMs rely on empirical phenology schemes that do not explicitly account for the mechanistic trade-offs between carbon gain and the avoidance of chilling or frost risk. Our R-OPT framework directly links phenological timing to these fundamental physiological trade-offs, providing a process-based alternative that is more mechanistically grounded than current empirical approaches. We therefore recommend the integration of a stand-alone phenological module, as represented by our R-OPT model, into ESMs to improve their representation of plant–environment interactions (Richardson et al., 2013). Furthermore, while many current ESMs are parameterized and validated at coarse spatial and temporal scales (Danabasoglu et al., 2020; Semmler et al., 2020), the growing availability of multi-decadal, large-scale phenological and plant trait datasets enables more robust evaluation and constraint of

model predictions. Adoption of mechanistically improved phenology modules is expected to reduce uncertainties in simulating ecosystem carbon cycling, water fluxes and energy dynamics across various scales. Ultimately, such advancements will enhance the accuracy of regional and global climate projections (Ryu et al., 2019) and inform more effective strategies for large-scale initiatives, including national-scale carbon neutrality plans (Brown et al., 2021; Huovila et al., 2022; Tan et al., 2022) and global biodiversity conservation targets (Green et al., 2019; Xu et al., 2021) through improved management of conservation, afforestation and restoration efforts.

While our proposed R-OPT model regards spring phenology as an optimal plant strategy to maximize photosynthetic carbon gain while minimize chilling risk, several caveats remain in our study, each suggesting key future directions for development. Firstly, the R-OPT model necessarily simplifies the complex ecological and biological processes underlying phenological responses. For instance, the optimal temporal window for balancing carbon gain and chilling risk, a central promise of our model, remains debated in the literature (Clark et al., 2014; Gauzere et al., 2019) and is not explicitly resolved here. In addition, factors such as climate extremes (He et al., 2018; Ma et al., 2015), disturbance histories (Norman et al., 2017), and species interactions through resource competition, nutrient cycling and trophic interactions (Renner & Zohner, 2018; Thackeray et al., 2016) have been previously observed or hypothesized to influence spring phenology but are not considered here. Despite these limitations, our work captures a key mechanistic trade-off between carbon gain and chilling risk that governs spring phenology timing. Future research should build upon our work, incorporating additional data to explore other vital ecological and biological processes affecting spring phenology behaviours and process-based modelling. Similarly, considering other timescales of optimal acclimation duration (beyond using the current year's preseason duration in this study) and how it varies with species and environments could also add depth to our model.

Secondly, our testing for the optimality theory underlying spring phenology regulation relies solely on process modelling and rigorous statistical analysis. To more robustly test and refine this theoretical framework, future research should incorporate experimental and molecular approaches (Hänninen et al., 2019; Wolkovich et al., 2022). Controlled experiments in laboratory and field settings, combined with target molecular analyses, can generate direct evidence to validate and improve our model—particularly by elucidating species-specific sensitivities to environmental factors. Such experiments, employing both control and treatment groups, would enable systematic manipulation of environmental conditions and assessment of their individual and interactive effects on spring phenology (Chamberlain & Wolkovich, 2021). Furthermore, integrating molecular data would facilitate identification of genetic mechanisms and regulatory pathways underlying phenological responses across different environmental niches (Mazer et al., 2015). Together, these approaches would provide a mechanistic foundation to rigorously test the validity of our model and the optimality hypothesis, potentially revealing the extent to which observed phenological patterns are driven by adaptive trade-offs at both physiological and genetic levels.

Thirdly, accurate parameterization of the Farquhar–Medlyn model to simulate early-season plant photosynthetic carbon uptake requires a comprehensive set of physiological traits (i.e. V_{cmax}, J_{max} and g_1). Previous studies have reported significant variations of these traits across plant species and growth environments (Lin et al., 2015; Yan et al., 2023). However, due to a lack of relevant data across the species-site level, we currently use a fixed set of values (such as constant photosynthetic parameters) in our model. Although our sensitivity analysis indicates a minimal impact of these fixed values in modelling intra-site decadal spring phenology dynamics (Figure S1), a more accurate representation of trait values across species and growth environments could improve the detailed mechanisms of species-specific phenological response to broader spatial or phylogenetic contexts. Trait variability across ecosystems—especially in non-European or phylogenetically diverse forest systems—may significantly affect model accuracy and generalizability (Westerband et al., 2021; Wong & Carmona, 2021; Zhou et al., 2022). Future studies should not only prioritize collecting more species- and site-specific trait data, but also focus on integrating emerging trait databases and remote sensing tools (with improved phenology monitoring across space and time). These approaches offer new opportunities to scale trait variation beyond Europe and provide a stronger foundation for assessing phenological optimality trade-offs, where parameters such as *a*, *b* and *c* may reflect underlying mechanisms across global ecosystems.

Taken together, these future directions may contribute to a more comprehensive understanding of plant phenology and its multifaceted responses to environmental changes. Advancing this research will help improve our ability to interpret ecosystem dynamics and inform more effective management and conservation strategies (Caparros-Santiago et al., 2021; Cleland et al., 2007; Ma et al., 2022; Richardson et al., 2010).

5 | CONCLUSIONS

In this study, we developed a new, theory-based spring phenology model and assessed the performance of both existing and newly proposed models for five major plant species across extensive spatial extents and decadal time durations in Europe. Our findings indicate that incorporating the Farquhar–Medlyn photosynthesis model into the current OPT model (or R-OPT) substantially improves the accuracy of spring phenology predictions, reducing the median RMSE from 7.91 days in the OPT model to 7.61 days in the R-OPT model. This improvement proved to be far more effective compared to the CFT (8.99 days) and GDD (8.97 days) models. A subsequent comprehensive cross-model comparison also confirmed the superiority of the optimality-based approach (i.e. R-OPT and OPT) over the non-optimality approach (i.e. CFT and GDD) in modelling spring phenology. From these analyses, we can infer two main points: (1) Spring phenology can be viewed as an optimal strategy for plants

to maximize early growing-season plant photosynthesis gains while minimizing chilling risk, and thus the optimality-based approach outperforms the non-optimality-based approach; (2) the Farquhar–Medlyn photosynthesis model offers an improved method to represent early growing-season photosynthetic carbon gain in R-OPT compared to the original OPT model (relying on photoperiods and forcing for approximation), thereby improving process-based modelling. Furthermore, we conducted an analysis of the geographical distribution of the paired model performance differences, which disclosed that the R-OPT model significantly outperformed the OPT model at northern, low-altitude sites compared to southern sites. In other words, the newly proposed R-OPT demonstrated markedly better performance than the default OPT model in low-latitude or high MAP areas, whereas its performance remained neutral in other regions. This difference could be due to increasing environmental constraints or an incomplete representation of photosynthetic carbon gain in high-latitude and environmentally harsher areas, which further undermines the effectiveness of R-OPT in simulating spring phenology compared to OPT in these regions. Consequently, a more thorough exploration of this issue is required in future studies. Collectively, these results enhance our understanding of plant spring phenological dynamics across species, space and time, shedding light on the fundamental theory underlying spring phenology regulation and model representation, thereby improving evaluations of many phenology-related ecological processes and their sensitivity response to climate change.

AUTHOR CONTRIBUTIONS

Jin Wu, Yating Gu, and Matteo Detto designed the study. Yating Gu and Zejun Wu carried out all the data analyses, and Jin Wu participated in the result interpretation. Yating Gu drafted the paper with constructive input from Jin Wu, and Yating Gu, Zejun Wu, Matteo Detto, Dedi Yang, Jiayue Wang, Yingyi Zhao, Xi Yang and Jin Wu contributed to the revision of the manuscript. Yating Gu and Zejun Wu co-contributed to this article.

ACKNOWLEDGEMENTS

This work was supported by the National Natural Science Foundation of China (#31922090) and the Hong Kong Research Grant Council General Research Fund (#17305321). Y. Gu was supported by the Natural Science Foundation of Jiangsu Province (Grant No. SBK20250403215). J. Wu was also supported by the HKU Seed Funding for Strategic Interdisciplinary Research Scheme, the Hong Kong Research Grant Council Collaborative Research Fund (#C5062-21GF) and the Innovation and Technology Fund (funding support to State Key Laboratory of Agrobiotechnology). D. Yang was supported by the Next-Generation Ecosystem Experiments (NGEE Arctic) project that is supported by The Office of Biological and Environmental Research in the United States Department of Energy, Office of Science and the Laboratory Directed Research and Development Program of Oak Ridge National Laboratory, managed by UT-Battelle, LLC, for the U.S. Department of Energy.

CONFLICT OF INTEREST STATEMENT

The authors declare that they have no known competing financial interests or personal relationships that could have appeared to influence the work reported in this paper.

PEER REVIEW

The peer review history for this article is available at https://www.webofscience.com/api/gateway/wos/peer-review/10.1111/2041-210X.70181.

DATA AVAILABILITY STATEMENT

All data needed to evaluate the conclusions of this paper are available via https://doi.org/10.6084/m9.figshare.30283042.v1 (Gu et al., 2025).

ORCID

Yating Gu https://orcid.org/0000-0001-8312-2473
Jin Wu https://orcid.org/0000-0001-8991-3970

REFERENCES

Anderegg, W. R. L., Wolf, A., Arango-Velez, A., Choat, B., Chmura, D. J., Jansen, S., Kolb, T., Li, S., Meinzer, F., Pita, P., Resco de Dios, V., Sperry, J. S., Wolfe, B. T., & Pacala, S. (2017). Plant water potential improves prediction of empirical stomatal models. *PLoS One*, *12*, e0185481.

Atkin, O. K., Bloomfield, K. J., Reich, P. B., Tjoelker, M. G., Asner, G. P., Bonal, D., Bönisch, G., Bradford, M. G., Cernusak, L. A., Cosio, E. G., Creek, D., Crous, K. Y., Domingues, T. F., Dukes, J. S., Egerton, J. J. G., Evans, J. R., Farquhar, G. D., Fyllas, N. M., Gauthier, P. P. G., … Zaragoza-Castells, J. (2015). Global variability in leaf respiration in relation to climate, plant functional types and leaf traits. *New Phytologist*, *206*, 614–636.

Badeck, F.-W., Bondeau, A., Böttcher, K., Doktor, D., Lucht, W., Schaber, J., & Sitch, S. (2004). Responses of spring phenology to climate change. *New Phytologist*, *162*, 295–309.

Brown, M. A., Dwivedi, P., Mani, S., Matisoff, D., Mohan, J. E., Mullen, J., Oxman, M., Rodgers, M., Simmons, R., & Beasley, B. (2021). A framework for localizing global climate solutions and their carbon reduction potential. *Proceedings of the National Academy of Sciences of the United States of America*, *118*, e2100008118.

Buckley, T. N. (2005). The control of stomata by water balance. *New Phytologist*, *168*, 275–292.

Buermann, W., Forkel, M., O'Sullivan, M., Sitch, S., Friedlingstein, P., Haverd, V., Jain, A. K., Kato, E., Kautz, M., Lienert, S., Lombardozzi, D., Nabel, J. E. M. S., Tian, H., Wiltshire, A. J., Zhu, D., Smith, W. K., & Richardson, A. D. (2018). Widespread seasonal compensation effects of spring warming on northern plant productivity. *Nature*, *562*, 110–114.

Caffarra, A., & Donnelly, A. (2011). The ecological significance of phenology in four different tree species: Effects of light and temperature on bud burst. *International Journal of Biometeorology*, *55*(5), 711–721. https://doi.org/10.1007/s00484-010-0386-1

Caparros-Santiago, J. A., Rodriguez-Galiano, V., & Dash, J. (2021). Land surface phenology as indicator of global terrestrial ecosystem dynamics: A systematic review. *ISPRS Journal of Photogrammetry and Remote Sensing*, *171*, 330–347.

Chamberlain, C. J., & Wolkovich, E. M. (2021). Late spring freezes coupled with warming winters alter temperate tree phenology and growth. *New Phytologist*, *231*, 987–995.

Cheng, M., Jin, J., & Jiang, H. (2021). Strong impacts of autumn phenology on grassland ecosystem water use efficiency on the Tibetan Plateau. *Ecological Indicators*, *126*, 107682.

Chmura, H. E., Kharouba, H. M., Ashander, J., Ehlman, S. M., Rivest, E. B., & Yang, L. H. (2019). The mechanisms of phenology: The patterns and processes of phenological shifts. *Ecological Monographs*, *89*, e01337.

Chuine, I. (2000). A unified model for budburst of trees. *Journal of Theoretical Biology*, *207*, 337–347.

Clark, J. S., Salk, C., Melillo, J., & Mohan, J. (2014). Tree phenology responses to winter chilling, spring warming, at north and south range limits. *Functional Ecology*, *28*, 1344–1355.

Cleland, E. E., Chuine, I., Menzel, A., Mooney, H. A., & Schwartz, M. D. (2007). Shifting plant phenology in response to global change. *Trends in Ecology & Evolution*, *22*, 357–365.

Cohen, J. M., Lajeunesse, M. J., & Rohr, J. R. (2018). A global synthesis of animal phenological responses to climate change. *Nature Climate Change*, *8*, 224–228.

Cook, B. I., Wolkovich, E. M., Davies, T. J., Ault, T. R., Betancourt, J. L., Allen, J. M., Bolmgren, K., Cleland, E. E., Crimmins, T. M., Kraft, N. J. B., Lancaster, L. T., Mazer, S. J., McCabe, G. J., McGill, B. J., Parmesan, C., Pau, S., Regetz, J., Salamin, N., Schwartz, M. D., & Travers, S. E. (2012). Sensitivity of spring phenology to warming across temporal and spatial climate gradients in two independent databases. *Ecosystems*, *15*, 1283–1294.

Danabasoglu, G., Lamarque, J.-F., Bacmeister, J., Bailey, D. A., DuVivier, A. K., Edwards, J., Emmons, L. K., Fasullo, J., Garcia, R., Gettelman, A., Hannay, C., Holland, M. M., Large, W. G., Lauritzen, P. H., Lawrence, D. M., Lenaerts, J. T. M., Lindsay, K., Lipscomb, W. H., Mills, M. J., … Strand, W. G. (2020). The community earth system model version 2 (CESM2). *Journal of Advances in Modeling Earth Systems*, *12*, e2019MS001916.

De Réaumur, R. (1735). Observations du thermomere. *Memories Academie Royale Sciences Paris*, 545–576.

Descals, A., Verger, A., Yin, G., Filella, I., Fu, Y. H., Piao, S., Janssens, I. A., & Peñuelas, J. (2022). Radiation-constrained boundaries cause nonuniform responses of the carbon uptake phenology to climatic warming in the Northern Hemisphere. *Global Change Biology*, *29*(3), 719–730. https://doi.org/10.1111/gcb.16502

Du, J., Li, K., He, Z., Chen, L., Lin, P., & Zhu, X. (2020). Daily minimum temperature and precipitation control on spring phenology in arid-mountain ecosystems in China. *International Journal of Climatology*, *40*, 2568–2579.

Fang, J., Shugart, H. H., Wang, L., Lutz, J. A., Yan, X., & Liu, F. (2024). Optimal representation of spring phenology on photosynthetic productivity across the northern hemisphere forests. *Agricultural and Forest Meteorology*, *350*, 109975.

Farquhar, G. D., von Caemmerer, S.v., & Berry, J. A. (1980). A biochemical model of photosynthetic CO_2 assimilation in leaves of C3 species. *Planta*, *149*, 78–90.

Forsythe, W. C., Rykiel, E. J., Stahl, R. S., Wu, H., & Schoolfield, R. M. (1995). A model comparison for daylength as a function of latitude and day of year. *Ecological Modelling*, *80*(1), 87–95. https://doi.org/10.1016/0304-3800(94)00034-f

Franks, P. J., Herold, N., Bonan, G. B., Oleson, K. W., Dukes, J. S., Huber, M., Schroeder, J. I., Cox, P. M., & Jones, S. (2024). Land surface conductance linked to precipitation: Co-evolution of vegetation and climate in Earth system models. *Global Change Biology*, *30*, e17188.

Fu, Y. H., Zhang, X., Piao, S., Hao, F., Geng, X., Vitasse, Y., Zohner, C., Peñuelas, J., & Janssens, I. A. (2019). Daylength helps temperate deciduous trees to leaf-out at the optimal time. *Global Change Biology*, *25*, 2410–2418.

Fu, Y. H., Zhao, H., Piao, S., Peaucelle, M., Peng, S., Zhou, G., Ciais, P., Huang, M., Menzel, A., Peñuelas, J., Song, Y., Vitasse, Y., Zeng, Z., & Janssens, I. A. (2015). Declining global warming effects on the phenology of spring leaf unfolding. *Nature*, *526*, 104–107.

Gallinat, A. S., Ellwood, E. R., Heberling, J. M., Miller-Rushing, A. J., Pearse, W. D., & Primack, R. B. (2021). Macrophenology: Insights into the broad-scale patterns, drivers, and consequences of phenology. *American Journal of Botany*, *108*, 2112–2126.

Garcia-Forner, N., Adams, H. D., Sevanto, S., Collins, A. D., Dickman, L. T., Hudson, P. J., Zeppel, M. J., Jenkins, M. W., Powers, H., & Martínez-Vilalta, J. (2016). Responses of two semiarid conifer tree species to reduced precipitation and warming reveal new perspectives for stomatal regulation. *Plant, Cell & Environment*, *39*, 38–49.

Gauzere, J., Lucas, C., Ronce, O., Davi, H., & Chuine, I. (2019). Sensitivity analysis of tree phenology models reveals increasing sensitivity of their predictions to winter chilling temperature and photoperiod with warming climate. *Ecological Modelling*, *411*, 108805.

Green, E. J., Buchanan, G. M., Butchart, S. H., Chandler, G. M., Burgess, N. D., Hill, S. L., & Gregory, R. D. (2019). Relating characteristics of global biodiversity targets to reported progress. *Conservation Biology*, *33*, 1360–1369.

Gu, Y., Meng, L., Wang, Y., Wu, Z., Pan, Y., Zhao, Y., Detto, M., & Wu, J. (2025). Uncovering the role of solar radiation and water stress factors in constraining decadal intra-site spring phenology variability in diverse ecosystems across the Northern Hemisphere. *New Phytologist*, *246*(5), 1986–2003.

Gu, Y., Zhao, Y., Guo, Z., Meng, L., Zhang, K., Wang, J., Lee, C. K. F., Xie, J., Wang, Y., Yan, Z., Zhang, H., & Wu, J. (2023). The underappreciated importance of solar radiation in constraining spring phenology of temperate ecosystems in the Northern and Eastern United States. *Remote Sensing of Environment*, *294*, 113617.

Gu, Y. (2025). Supporting data for 'Improving leaf spring phenology modeling for temperate tree species: An integration of the Farquhar-Medlyn photosynthesis model with the optimality-based approach'. *figshare*, https://doi.org/10.6084/m9.figshare.30283042.v1

Guo, Z., Yan, Z., Majcher, B. M., Lee, C. K., Zhao, Y., Song, G., Wang, B., Wang, X., Deng, Y., & Michaletz, S. T. (2022). Dynamic biotic controls of leaf thermoregulation across the diel timescale. *Agricultural and Forest Meteorology*, *315*, 108827.

Han, W., Prentice, I. C., Tyler, W. D., Trevor, F. K., Ian, J. W., & Changhui, P. (2017). Photosynthetic responses to altitude an explanation based on optimality principles. *The New Phytologist*, *213*, 976–982.

Hänninen, H. (1990). Modelling bud dormancy release in trees from cool and temperate regions. *Acta Forestalia Fennica*, *213*, 7660.

Hänninen, H., Kramer, K., Tanino, K., Zhang, R., Wu, J., & Fu, Y. H. (2019). Experiments are necessary in process-based tree phenology modelling. *Trends in Plant Science*, *24*, 199–209.

He, Z., Du, J., Chen, L., Zhu, X., Lin, P., Zhao, M., & Fang, S. (2018). Impacts of recent climate extremes on spring phenology in arid-mountain ecosystems in China. *Agricultural and Forest Meteorology*, *260*, 31–40.

Hernández, G. G., Winter, K., & Slot, M. (2020). Similar temperature dependence of photosynthetic parameters in sun and shade leaves of three tropical tree species. *Tree Physiology*, *40*, 637–651.

Hua, X., Ohlemüller, R., & Sirguey, P. (2022). Differential effects of topography on the timing of the growing season in mountainous grassland ecosystems. *Environmental Advances*, *8*, 100234.

Huovila, A., Siikavirta, H., Rozado, C. A., Rökman, J., Tuominen, P., Paiho, S., Hedman, Å., & Ylén, P. (2022). Carbon-neutral cities: Critical review of theory and practice. *Journal of Cleaner Production*, *341*, 130912.

Kim, S., Kim, T. K., Yoon, S., Jang, K., Chun, J.-H., Won, M., Lim, J.-H., & Kim, H. S. (2022). Quantifying the importance of day length in process-based models for the prediction of temperate spring flowering phenology. *Science of the Total Environment*, *843*, 156780.

Kolassa, J., Reichle, R. H., Koster, R. D., Liu, Q., Mahanama, S., & Zeng, F.-W. (2020). An observation-driven approach to improve vegetation phenology in a global land surface model. *Journal of Advances in Modeling Earth Systems*, *12*, e2020MS002083.

Lieth, H. (2013). *Phenology and seasonality modeling*. Springer Science & Business Media.

Lin, Y.-S., Medlyn, B. E., Duursma, R. A., Prentice, I. C., Wang, H., Baig, S., Eamus, D., de Dios, V. R., Mitchell, P., Ellsworth, D. S., de Beeck, M. O., Wallin, G., Uddling, J., Tarvainen, L., Linderson, M.-L., Cernusak, L. A., Nippert, J. B., Ocheltree, T. W., Tissue, D. T., … Wingate, L. (2015). Optimal stomatal behaviour around the world. *Nature Climate Change*, *5*, 459–464.

Lundell, R., Hänninen, H., Saarinen, T., Åström, H., & Zhang, R. (2020). Beyond rest and quiescence (endodormancy and ecodormancy): A novel model for quantifying plant–environment interaction in bud dormancy release. *Plant, Cell & Environment*, *43*, 40–54.

Ma, X., Huete, A., Moran, S., Ponce-Campos, G., & Eamus, D. (2015). Abrupt shifts in phenology and vegetation productivity under climate extremes. *Journal of Geophysical Research: Biogeosciences*, *120*, 2036–2052.

Ma, X., Zhu, X., Xie, Q., Jin, J., Zhou, Y., Luo, Y., Liu, Y., Tian, J., & Zhao, Y. (2022). Monitoring nature's calendar from space: Emerging topics in land surface phenology and associated opportunities for science applications. *Global Change Biology*, *28*, 7186–7204.

Mazer, S. J., Gerst, K. L., Matthews, E. R., & Evenden, A. (2015). Species-specific phenological responses to winter temperature and precipitation in a water-limited ecosystem. *Ecosphere*, *6*, 1–27.

McMaster, G. S., & Wilhelm, W. (1997). Growing degree-days: One equation, two interpretations. *Agricultural and Forest Meteorology*, *87*, 291–300.

Medlyn, B. E., Dreyer, E., Ellsworth, D., Forstreuter, M., Harley, P. C., Kirschbaum, M. U. F., Le Roux, X., Montpied, P., Strassemeyer, J., Walcroft, A., Wang, K., & Loustau, D. (2002). Temperature response of parameters of a biochemically based model of photosynthesis. II. A review of experimental data. *Plant, Cell & Environment*, *25*, 1167–1179.

Medlyn, B. E., Duursma, R. A., Eamus, D., Ellsworth, D. S., Prentice, I. C., Barton, C. V., Crous, K. Y., De Angelis, P., Freeman, M., & Wingate, L. (2011). Reconciling the optimal and empirical approaches to modelling stomatal conductance. *Global Change Biology*, *17*, 2134–2144.

Meng, L., Zhou, Y., Gu, L., Richardson, A. D., Peñuelas, J., Fu, Y., Wang, Y., Asrar, G. R., De Boeck, H. J., & Mao, J. (2021). Photoperiod decelerates the advance of spring phenology of six deciduous tree species under climate warming. *Global Change Biology*, *27*, 2914–2927.

Miller, D. L., Wolf, S., Fisher, J. B., Zaitchik, B. F., Xiao, J., & Keenan, T. F. (2023). Increased photosynthesis during spring drought in energy-limited ecosystems. *Nature Communications*, *14*, 7828.

Mo, Y., Li, X., Guo, Y., & Fu, Y. (2023). Warming increases the differences among spring phenology models under future climate change. *Frontiers in Plant Science*, *14*, 1266801.

Navarro, J., Powers, J. M., Paul, A., & Campbell, D. R. (2022). Phenotypic plasticity and selection on leaf traits in response to snowmelt timing and summer precipitation. *New Phytologist*, *234*, 1477–1490.

Nehemy, M. F., Pierrat, Z., Maillet, J., Richardson, A. D., Stutz, J., Johnson, B., Helgason, W., Barr, A. G., Laroque, C. P., & McDonnell, J. J. (2023). Phenological assessment of transpiration: The stem-temp approach for determining start and end of season. *Agricultural and Forest Meteorology*, *331*, 109319.

Norman, S. P., Hargrove, W. W., & Christie, W. M. (2017). Spring and autumn phenological variability across environmental gradients of Great Smoky Mountains National Park, USA. *Remote Sensing*, *9*, 407.

Ofori-Amanfo, K. K., Klem, K., Veselá, B., Holub, P., Agyei, T., Marek, M. V., Grace, J., & Urban, O. (2020). Interactive effect of elevated CO_2 and reduced summer precipitation on photosynthesis is species-specific: The case study with soil-planted Norway spruce and sessile oak in a mountainous forest plot. *Forests*, *12*, 42.

Piao, S., Liu, Q., Chen, A., Janssens, I. A., Fu, Y., Dai, J., Liu, L., Lian, X., Shen, M., & Zhu, X. (2019). Plant phenology and global climate change: Current progresses and challenges. *Global Change Biology*, *25*, 1922–1940.

Prevéy, J., Vellend, M., Rüger, N., Hollister, R. D., Bjorkman, A. D., Myers-Smith, I. H., Elmendorf, S. C., Clark, K., Cooper, E. J., Elberling, B., Fosaa, A. M., Henry, G. H. R., Høye, T. T., Jónsdóttir, I. S., Klanderud, K., Lévesque, E., Mauritz, M., Molau, U., Natali, S. M., … Rixen, C. (2017). Greater temperature sensitivity of plant phenology at colder sites: Implications for convergence across northern latitudes. *Global Change Biology*, *23*, 2660–2671.

Renner, S. S., & Zohner, C. M. (2018). Climate change and phenological mismatch in trophic interactions among plants, insects, and vertebrates. *Annual Review of Ecology, Evolution, and Systematics*, *49*, 165–182.

Richardson, A. D., Andy Black, T., Ciais, P., Delbart, N., Friedl, M. A., Gobron, N., Hollinger, D. Y., Kutsch, W. L., Longdoz, B., Luyssaert, S., Migliavacca, M., Montagnani, L., William Munger, J., Moors, E., Piao, S., Rebmann, C., Reichstein, M., Saigusa, N., Tomelleri, E., … Varlagin, A. (2010). Influence of spring and autumn phenological transitions on forest ecosystem productivity. *Philosophical Transactions of the Royal Society, B: Biological Sciences*, *365*, 3227–3246.

Richardson, A. D., Keenan, T. F., Migliavacca, M., Ryu, Y., Sonnentag, O., & Toomey, M. (2013). Climate change, phenology, and phenological control of vegetation feedbacks to the climate system. *Agricultural and Forest Meteorology*, *169*, 156–173.

Ryu, Y., Berry, J. A., & Baldocchi, D. D. (2019). What is global photosynthesis? History, uncertainties and opportunities. *Remote Sensing of Environment*, *223*, 95–114.

Sapkota, S., Salem, M., Jahed, K. R., Artlip, T. S., & Sherif, S. M. (2023). From endodormancy to ecodormancy: The transcriptional landscape of apple floral buds. *Frontiers in Plant Science*, *14*, 1194244.

Scheifinger, H., Hübner, T., Koch, E., Paul, A., & Ungersböck, M. (2018). A European phenological database, PEP725, www.pep725.eu. *EGU General Assembly Conference Abstracts* (p. 8578)

Schrodt, F., De La Barreda Bautista, B., Williams, C., Boyd, D. S., Schaepman-Strub, G., & Santos, M. J. (2020). Integrating biodiversity, remote sensing, and auxiliary information for the study of ecosystem functioning and conservation at large spatial scales. In J. Cavender-Bares, J. A. Gamon, & P. A. Townsend (Eds.), *Remote sensing of plant biodiversity* (pp. 449–484). Springer.

Semmler, T., Danilov, S., Gierz, P., Goessling, H. F., Hegewald, J., Hinrichs, C., Koldunov, N., Khosravi, N., Mu, L., Rackow, T., Sein, D. V., Sidorenko, D., Wang, Q., & Jung, T. (2020). Simulations for CMIP6 with the AWI climate model AWI-CM-1-1. *Journal of Advances in Modeling Earth Systems*, *12*, e2019MS002009.

Tan, X.-C., Kong, L.-S., Gu, B.-H., Zeng, A., & Niu, M.-M. (2022). Research on the carbon neutrality governance under a polycentric approach. *Advances in Climate Change Research*, *13*, 159–168.

Templ, B., Koch, E., Bolmgren, K., Ungersböck, M., Paul, A., Scheifinger, H., Rutishauser, T., Busto, M., Chmielewski, F.-M., & Hájková, L. (2018). Pan European Phenological database (PEP725): A single point of access for European data. *International Journal of Biometeorology*, *62*, 1109–1113.

Thackeray, S. J., Henrys, P. A., Hemming, D., Bell, J. R., Botham, M. S., Burthe, S., Helaouet, P., Johns, D. G., Jones, I. D., & Leech, D. I. (2016). Phenological sensitivity to climate across taxa and trophic levels. *Nature*, *535*, 241–245.

Tian, F., Cai, Z., Jin, H., Hufkens, K., Scheifinger, H., Tagesson, T., Smets, B., Van Hoolst, R., Bonte, K., & Ivits, E. (2021). Calibrating vegetation phenology from Sentinel-2 using eddy covariance, PhenoCam, and PEP725 networks across Europe. *Remote Sensing of Environment*, *260*, 112456.

Wang, H., Wu, C., Ciais, P., Peñuelas, J., Dai, J., Fu, Y., & Ge, Q. (2020). Overestimation of the effect of climatic warming on spring phenology due to misrepresentation of chilling. *Nature Communications*, *11*, 4945.

Wang, X., Wu, C., Peng, D., Gonsamo, A., & Liu, Z. (2018). Snow cover phenology affects alpine vegetation growth dynamics on the

Tibetan plateau: Satellite observed evidence, impacts of different biomes, and climate drivers. *Agricultural and Forest Meteorology*, *256–257*, 61–74.

Wang, X., Xiao, J., Li, X., Cheng, G., Ma, M., Zhu, G., Altaf Arain, M., Andrew Black, T., & Jassal, R. S. (2019). No trends in spring and autumn phenology during the global warming hiatus. *Nature Communications*, *10*, 2389.

Wang, X., Xu, H., Ma, Q., Luo, Y., He, D., Smith, N. G., Rossi, S., & Chen, L. (2023). Chilling and forcing proceed in parallel to regulate spring leaf unfolding in temperate trees. *Global Ecology and Biogeography*, *32*, 1914–1927.

Westerband, A. C., Funk, J. L., & Barton, K. E. (2021). Intraspecific trait variation in plants: A renewed focus on its role in ecological processes. *Annals of Botany*, *127*, 397–410.

Wolkovich, E., Chamberlain, C., Buonaiuto, D., Ettinger, A., & Morales-Castilla, I. (2022). Integrating experiments to predict interactive cue effects on spring phenology with warming. *New Phytologist*, *235*, 1719–1728.

Wong, M. K., & Carmona, C. P. (2021). Including intraspecific trait variability to avoid distortion of functional diversity and ecological inference: Lessons from natural assemblages. *Methods in Ecology and Evolution*, *12*, 946–957.

Wu, J., Serbin, S. P., Ely, K. S., Wolfe, B. T., Dickman, L. T., Grossiord, C., Michaletz, S. T., Collins, A. D., Detto, M., McDowell, N. G., Wright, S. J., & Rogers, A. (2020). The response of stomatal conductance to seasonal drought in tropical forests. *Global Change Biology*, *26*, 823–839.

Wu, J., Serbin, S. P., Xu, X., Albert, L. P., Chen, M., Meng, R., Saleska, S. R., & Rogers, A. (2017). The phenology of leaf quality and its within-canopy variation is essential for accurate modeling of photosynthesis in tropical evergreen forests. *Global Change Biology*, *23*, 4814–4827.

Xie, J., Hüsler, F., de Jong, R., Chimani, B., Asam, S., Sun, Y., Schaepman, M. E., & Kneubühler, M. (2021). Spring temperature and snow cover climatology drive the advanced springtime phenology (1991–2014) in the European Alps. *Journal of Geophysical Research – Biogeosciences*, *126*, e2020JG006150.

Xu, H., Cao, Y., Yu, D., Cao, M., He, Y., Gill, M., & Pereira, H. M. (2021). Ensuring effective implementation of the post-2020 global biodiversity targets. *Nature Ecology & Evolution*, *5*, 411–418.

Yan, Z., Guo, Z., Serbin, S. P., Song, G., Zhao, Y., Chen, Y., Wu, S., Wang, J., Wang, X., & Li, J. (2021). Spectroscopy outperforms leaf trait relationships for predicting photosynthetic capacity across different forest types. *New Phytologist*, *232*, 134–147.

Yan, Z., Sardans, J., Peñuelas, J., Detto, M., Smith, N. G., Wang, H., Guo, L., Hughes, A. C., Guo, Z., Lee, C. K. F., Liu, L., & Wu, J. (2023). Global patterns and drivers of leaf photosynthetic capacity: The relative importance of environmental factors and evolutionary history. *Global Ecology and Biogeography*, *32*, 668–682.

Yang, L. H., & Rudolf, V. (2010). Phenology, ontogeny and the effects of climate change on the timing of species interactions. *Ecology Letters*, *13*, 1–10.

Yuan, W., Zheng, Y., Piao, S., Ciais, P., Lombardozzi, D., Wang, Y., Ryu, Y., Chen, G., Dong, W., Hu, Z., Jain, A. K., Jiang, C., Kato, E., Li, S., Lienert, S., Liu, S., Nabel, J. E. M. S., Qin, Z., Quine, T., … Yang, S. (2019). Increased atmospheric vapor pressure deficit reduces global vegetation growth. Science. *Advances*, *5*(8), eaax1396. https://doi.org/10.1126/sciadv.aax1396

Zhou, J., Cieraad, E., & van Bodegom, P. M. (2022). Global analysis of trait–trait relationships within and between species. *New Phytologist*, *233*, 1643–1656.

Zhou, S., Duursma, R. A., Medlyn, B. E., Kelly, J. W. G., & Prentice, I. C. (2013). How should we model plant responses to drought? An analysis of stomatal and non-stomatal responses to water stress. *Agricultural and Forest Meteorology*, *182–183*, 204–214.

Zohner, C. M., Renner, S. S., Sebald, V., & Crowther, T. W. (2021). How changes in spring and autumn phenology translate into growth-experimental evidence of asymmetric effects. *Journal of Ecology*, *109*, 2717–2728.

SUPPORTING INFORMATION

Additional supporting information can be found online in the Supporting Information section at the end of this article.

Figure S1. Linear regression analysis between the model performance (RMSE, days) and two parameters (a: $V_{c,max25}$ ($\mu mol\,m^{-2}\,s^{-1}$); b: g_1 (-)) in selected species *Aesculus hippocastanum* (a, b), *Alnus glutinosa* (c, d), *Fagus sylvatica* (e, f), *Fraxinus excelsior* (g, h), *Sorbus aucuparia* (i, j). The other parameters were fixed (such as parameters a–c) and then randomly generated $V_{c,max25}$ ($\mu mol\,m^{-2}\,s^{-1}$) in the range [50, 80] and g_1 in the range [1, 5] to test the model's sensitivity to these two parameters for the selected species *Aesculus hippocastanum*. The results demonstrated minimal to no correlation between both parameters and the RMSE for selected species. The correlation coefficients were −0.002 for $V_{c,max25}$, 0.001 for g_1, with all *p*-values less than 0.05.

Figure S2. Schematic diagram illustrating the limitation framework of leaf photosynthesis. Net assimilation rate (A_n) is determined by the minimum of three potential limitations: the Rubisco-limited rate (A_c), the electron transport-limited rate (A_j) and the triose phosphate utilization (TPU)-limited rate (A_p). These rates are expressed in μmol CO_2 $m^{-2}\,s^{-1}$. The net rate also accounts for mitochondrial respiration in the light (R_d). In addition, stomatal conductance is regulated through parameters including the residual conductance to water vapour (g_0, mol $m^{-2}\,s^{-1}$), vapour pressure deficit (VPD, kPa), stomatal slope (g_1) and atmospheric CO_2 concentration (C_a, ppm). Together, these processes reflect the balance between carbon uptake and environmental constraints on photosynthesis.

Table S1. Modified equations of the Farquhar, von Caemmerer and Berry (FvCB; Farquhar et al., 1980) leaf photosynthesis model, coupled with Medlyn type stomatal conductance scheme (Medlyn et al., 2011).

How to cite this article: Gu, Y., Wu, Z., Detto, M., Yang, D., Wang, J., Zhao, Y., Yang, X., & Wu, J. (2025). Improving leaf spring phenology modelling for temperate tree species: An integration of the Farquhar–Medlyn photosynthesis model with the optimality-based approach. *Methods in Ecology and Evolution*, *16*, 2901–2918. https://doi.org/10.1111/2041-210X.70181